Nanoscale

RSC Publishing

PAPER

View Article Online
View Journal | View Issue

Cite this: *Nanoscale*, 2013, **5**, 9123

Microscopic bimetallic actuator based on a bilayer of graphene and graphene oxide†

Hengchang Bi,[a] Kuibo Yin,[a] Xiao Xie,[a] Yilong Zhou,[a] Shu Wan,[a] Florian Banhart[b] and Litao Sun*[a]

Received 22nd April 2013
Accepted 6th July 2013

DOI: 10.1039/c3nr01988h

www.rsc.org/nanoscale

We present an actuator, consisting of a bilayer of graphene and graphene oxide, which allows us to exert forces in micromechanical systems that are at least 50 times higher than reported for other actuators of comparable size. The durability of such a device and stability during many cycles are demonstrated, and the related mechanism is discussed in detail.

Introduction

Since graphene sheets were obtained through micromechanical exfoliation,[1] they have been investigated by many researchers because of their excellent mechanical and unique electronic properties.[2–4] According to previous publications, paper-like materials, such as those fabricated through the vacuum filtration of graphene suspensions, exhibit good mechanical properties, a hardness of about 217 kg f mm^{-2}, and a yield strength of about 6.4 TPa.[5,6] Graphene papers demonstrate outstanding bending rigidity and elastic modulus.[5] These superior mechanical properties indicate that graphene paper may be an excellent material for use in actuators. In addition, graphene oxide (G-O) is a layered material consisting of hydrophilic oxygenated graphene sheets (G-O sheets) with oxygen-bearing functional groups on their basal planes and edges.[7] Monolayer G-O has an effective Young's modulus of (207 ± 23.4) GPa.[8] G-O paper materials, which are obtained through a flow-directed assembly method, possess a unique layered structure, in which individual G-O nanosheets are cross-linked together. This unique structure endows G-O paper with good mechanical properties, including a modulus of about 40 GPa and a fracture strength of about 130 MPa.[9] All of these excellent mechanical properties make graphene an ideal material for high-performance actuators. Actuators based on carbon allotropes,[10–25] polymer,[26,27] or inorganic materials,[28–30] *etc.*, have attracted much attention, and shown a broad range of potential micro/nanoelectromechanical applications. Additionally, the use of two different building blocks as a means of fabricating asymmetric materials has been proven to be a useful approach for producing mechanical actuators.[18,31] However, these actuators either have a very small deflection[30,31] or possess low load capacity.[32,33] So fabricating the actuators with large deflection and high load capacity is still a challenge.

In the present study, we present an electrothermal actuator based on a bilayer of graphene and G-O. Both graphene and G-O papers have similar layered structures that are compatible for the formation of a stable interface between the two layers. Furthermore, while the two types of paper share close values of Young's modulus (40 GPa), their coefficients of thermal expansion are remarkably different.[7,34] The combination of these materials has the potential to yield high movement efficiency while maintaining a uniform stress force. Using bilayer actuators composed of graphene and G-O papers, we designed an applicable practical like "artificial cilia" to realize arbitrary, controllable lifts and movements of objects in a two-dimensional (2-D) plane, which shows great potential for applications in micro- and nano-electromechanical systems (MEMS and NEMS). More importantly, the bilayer actuators show at least 50 times higher load capacity (~10 mg per actuator) than those of other microconveyor systems (0.196 mg per actuator; 0.022 mg per actuator), and 14 times larger displacement than that of other actuators.[30–33]

Results and discussion

G-O sheets are metastable at room temperature.[35] To improve the stability of G-O papers, the as-obtained graphite oxide was annealed at 75 °C for 24 h before being used to form G-O dispersions. The bilayer paper was prepared by the sequential filtration of the graphene dispersion and the G-O suspension (Fig. 1a). Both surfaces of the circular bilayer paper were macroscopically flat. The filtration sequence of the graphene dispersion and the G-O suspension were determined by the

[a]SEU-FEI Nano-Pico Center, Key Laboratory of MEMS of Ministry of Education, Southeast University, Nanjing 210096, P. R. China. E-mail: slt@seu.edu.cn; Fax: +86-025-83792939; Tel: +86-025-83792632-8813

[b]Institut de Physique et Chimie des Matériaux, UMR 7504 CNRS, Université de Strasbourg, 23 rue du Loess, 67034 Strasbourg, France

† Electronic supplementary information (ESI) available: The tests of electrical properties of graphene paper and G-O paper, XRD patterns of graphene and G-O, IR spectra of graphene and G-O, the parameters of bilayer beams and the response of the beams to the temperature are described in the document. See DOI: 10.1039/c3nr01988h

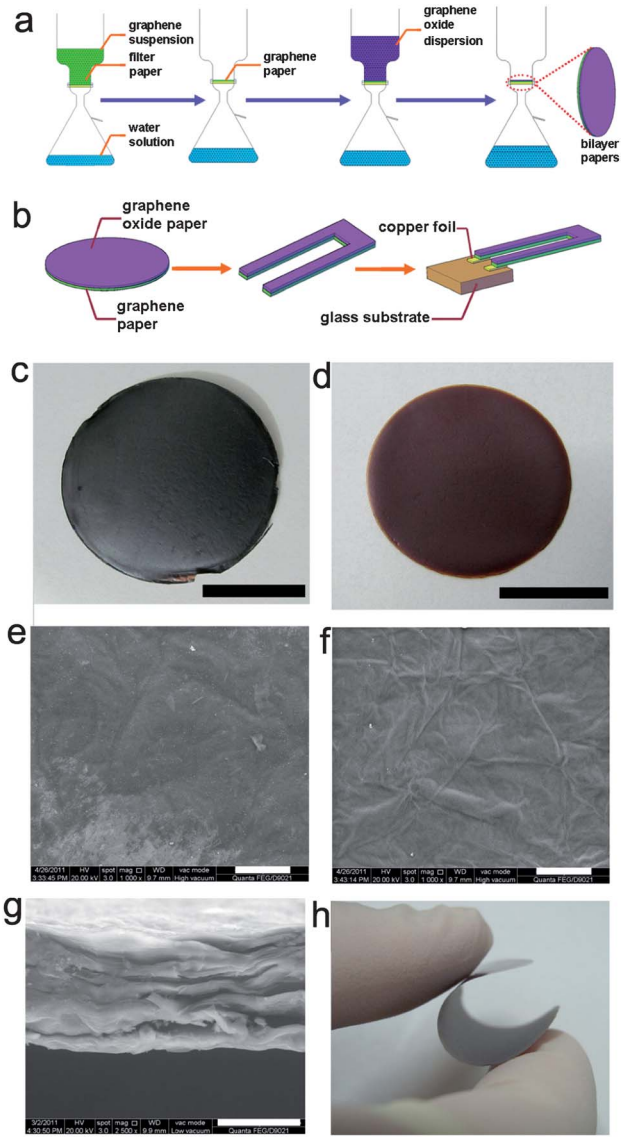

Fig. 1 Fabrication of the actuator and characterization of bilayer papers. (a) Bilayer paper was produced *via* the vacuum filtration of a graphene dispersion and a G-O suspension in sequence. (b) The bilayer paper was fabricated into an actuator using a sharp razor blade. (c) Digital photograph of the graphene side. Scale bar: 2 cm. (d) Digital photograph of the G-O side. Scale bar: 2 cm. (e) The surface of the graphene paper. Scale bar: 50 μm. (f) The surface of the G-O paper. Scale bar: 50 μm. (g) The cross-sectional morphology of the bilayer paper indicates a compact combination. Scale bar: 30 μm. (h) Bilayer papers are flexible.

hydrophobic nature of the graphene sheets and by the hydrophilic nature of the G-O sheets. In reverse sequential filtration, as-prepared G-O layers slightly disperse in water, inevitably causing indistinct boundaries between the two layers. An indistinct boundary would have an unfavourable effect on the outer surface of the G-O component. The thickness of each layer could be controlled by adjusting the concentration and volume of the suspensions and dispersions during filtration. The as-prepared bilayer paper was then cut into a series of U-shaped beams (Fig. 1b) using a sharp razor blade (Fig. 1b). Copper wires were joint with copper foils by electric welding. The copper foils were then attached to glass substrates followed by the attachment of the U-shaped beams to the copper foils using conductive adhesive to complete the assembly of an actuator.

Fig. 1c and d show digital photographs of the surface of the bilayer papers. The surface of the graphene paper was black (Fig. 1c) and electrically conductive (Fig. S1, ESI†). By contrast, the surface of the G-O paper was dark brown (Fig. 1d) and electrically insulating (Fig. S1, ESI†). In addition, scanning electron microscopy (SEM) was applied to characterize the surface and the cross-section of the bilayer papers (Fig. 1). More wrinkles were formed on the surface of the G-O paper (Fig. 1f) as compared to the surface of the graphene paper (Fig. 1e); such wrinkles roughened the G-O side. This phenomenon could be explained by two mechanisms. On the one hand, a large number of oxygen-containing functional groups, including carboxyl and hydroxyl groups, among others, bind to the G-O sheets, thereby preventing compact integration. On the other hand, the surface morphology of the filter paper exhibited significant effects on the surface of the graphene layer. The thickness and cross-sectional morphology of the bilayer paper were determined by SEM. The interface between the graphene and G-O layers was difficult to be determined (Fig. 1g). The cross-sections of each layer in the bilayer paper sample demonstrated the same morphology as in individually prepared G-O and graphene papers.[9,36] The bilayer paper was not delaminated to any extent, which was beneficial for the fabrication of the paper and its application in an actuator. To measure the individual thickness of the graphene and G-O papers of the bilayer accurately, we made additional graphene and G-O papers using vacuum filtration. The concentration and volume of graphene dispersions and G-O suspensions were the same as those used in the fabrication of the bilayer papers. The bilayer papers showed good mechanical properties, including excellent flexibility (Fig. 1f). They could be bent at any angle. Differences in the surface morphology, thermal expansion coefficient, basal spacing (Fig. S2, ESI†), and electrical properties between the graphene and G-O papers may be attributed to the oxygen-containing functional groups found on the G-O sheets. Very few of such groups could be found on the graphene sheets (Fig. S3, ESI†).

We investigated the action of bilayer papers as a function of an applied voltage at room temperature. The free end of a U-shaped beam curled upward depending on the voltage (Fig. 2b). In addition, a threshold voltage was observed. At the threshold, the displacement of the beam was negligible. At relatively low voltages, the beam rolled toward the face of the G-O layer. As the voltage was increased, the beam rolled up further with higher curvature (defined as the reciprocal of the radius) (Fig. S4, ESI†). The beam gradually unrolled and returned to its original shape (Fig. 2c) after the power supply was switched off. This dynamic process is shown in the ESI (Video 1†).

A series of bilayer papers with the same graphene layer thicknesses but with different G-O layer thicknesses was fabricated. The bilayer papers were cut into the same U-shaped beams and then assembled into the same actuators. Fig. 2d demonstrates that the displacement of these beams was a function of the applied voltage. As the threshold voltage varies

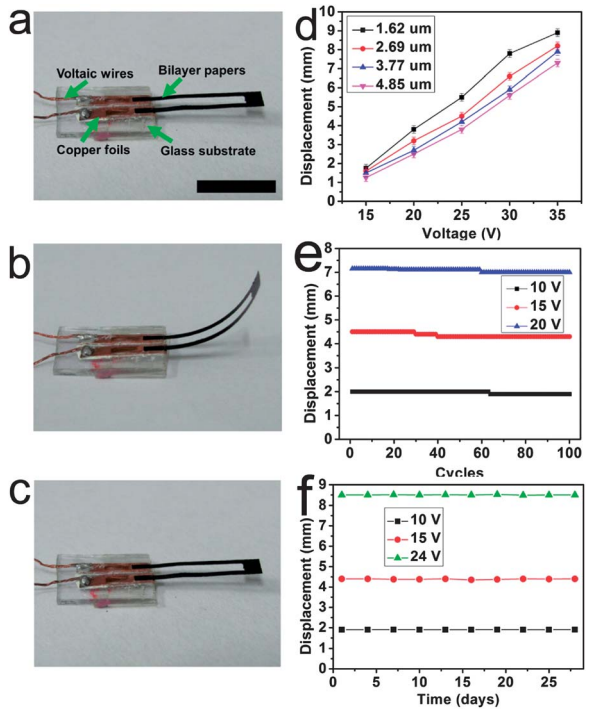

Fig. 2 The as-fabricated actuator and the performance of a full graphene actuator. (a) Every component of the actuator was marked, and the beam was initially flat. Scale bar: 1 cm. (b) Curling was observed after the power was switched on. (c) The beam unrolled and returned to its original shape (a) when the power was cut off. (d) Four actuators (lengths of ~17 mm) with the same graphene paper thickness of ~3.61 μm but different G-O paper thicknesses (*i.e.*, 1.62, 2.69, 3.77, and 4.85 μm) demonstrated a linear change in displacement as the voltage varied. (e) The durability of the devices over 100-cycle tests at 10, 15, and 20 V. (f) The stability of the actuators over one month. The actuator used to test durability and stability had a length of ~15 mm, a total width of ~1.8 mm, and a total thickness of ~7.38 μm (graphene paper ~3.61 μm, G-O paper ~3.77 μm).

slightly with the thickness of the G-O layers, only comparable data that were higher than the threshold were studied in the present work.

The displacement increased as the voltage increased for all the beams, and the displacement of the beams with thinner G-O layers was larger than that of the beams with thicker G-O layers under the same testing voltage. The displacement of the actuator with thinner G-O layers can be up to 9 mm, which is ~14 times higher than that of other actuator with comparative size.[31] Moreover, a linear relationship between the displacement of the free end of the beam and the applied voltage was observed. The durability of the actuators after several cycles and their stability over time were also investigated. Fig. 2e demonstrates that the displacement of the actuator decreased by only ~5%, ~7%, and ~3% over 100 measurement cycles at 10, 15, and 20 V, respectively, indicating sufficiently stable responses of the actuators based on the bilayer papers. As shown in Fig. 2f, the actuators were tested repeatedly every 3 days for a month at 10, 15, and 24 V. The displacement of the actuators at various voltages fluctuated slightly with time. The data showed good consistency, indicating that actuators based on graphene/G-O papers perform well and possess good stability. This finding is consistent with that in the literature.[37,38] Meanwhile, by using the micromolding in capillary methodology,[39] the actuators can shrink down to smaller size, with thickness of a few nanometers, width of a few micrometers, and length of sub-millimeter range.

According to previous literature,[18] the actuation of beams may be attributed to the internal heat generated by the current (Joule heat). To verify that the curling of the beam was a function of temperature, a thermal infrared imager was employed to monitor temperature changes of the beam surface under different testing voltages (Fig. 3). From the thermal infrared images, at least two important clues can clearly be obtained. On the one hand, with the increase of the testing voltage, the temperature of the beam rises gradually leading to greater displacement, which is in accordance with Fig. 2d. On the other hand, the temperature only reaches 62 °C despite the increase of the testing voltage to 40 V. As shown in the results in Fig. 2e, the thermal reduction of the G-O paper under the working voltages is not a concern. In addition, the actuators were inserted into a drying oven wherein the temperature can be controlled. The beam started to curl as expected (Fig. S5, ESI†).

The significant difference in the thermal expansion between graphene and G-O stems from their completely different surface chemistry, as stated above (Fig. S2 and S3, ESI†). For U-shaped beams, the G-O layer showed the lowest electrical conductivity while the graphene layer showed a resistance of several thousand ohms. These layers could generate a large amount of heat when an electric current passes through them, causing a rise in local temperature.

Consequently, a significant thermal stress prevails at the interface between graphene and G-O. In addition, the rise in temperature of the G-O layer may be conducted through heat transfer, which could generate a temperature gradient across the interface. As early as 1925, Timoshenko[40] studied bi-metal thermostats, in which the thermal stress between two metal

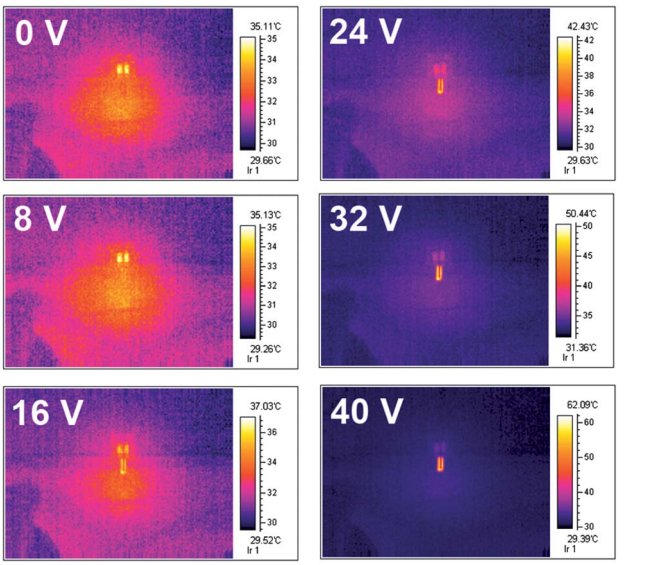

Fig. 3 Thermal infrared images of the U-shaped beam tested under different voltages ranging from 0 V to 40 V. The temperature of the beam rose gradually as the testing voltage increased steadily.

films was considered to be the main reason for the bending. However, data on full-graphene actuators were not available to date.

To quantify the function of the actuator, a classical model for bilayer beams was adopted,[41] as shown in eqn (1).

$$\frac{1}{r} = \frac{6w_1w_2E_1E_2t_1t_2(t_1+t_2)(\alpha_1-\alpha_2)\Delta T}{(w_1E_1t_1^2)^2+(w_2E_2t_2^2)^2+2w_1w_2E_1E_2t_1t_2(2t_1^2+3t_1t_2+2t_2^2)} \quad (1)$$

where t_1, w_1, α_1, and E_1 are the thickness, width, thermal expansion coefficient, and Young's modulus of the G-O layer, respectively. The symbols t_2, w_2, α_2, and E_2 are the corresponding parameters of the graphene layer. The symbols l, r, and ΔT represent the length, radius of curvature, and the difference between the initial temperature and the final temperature of the macroactuator, respectively. The parameters of the beam are provided in ESI, Fig. S4.† For a given macroactuator, l and w are the same for both the graphene and G-O papers. Thus, eqn (1) can be simplified to eqn (2). The curvature of the beam is proportional to ΔT. In addition, the greater the difference between α_1 and α_2, the greater the displacement of the free end of the beam under the same conditions. According to the literature, graphene and G-O papers have nearly equal values of Young's modulus, allowing eqn (2) to be simplified to eqn (3). The curvature of the beam can be related to three parameters, namely thickness, thermal expansion coefficient of each paper, and final temperature difference. Thus, the combination of graphene/G-O papers is a very favourable choice for many applications.

$$\frac{1}{r} = \frac{6E_1E_2t_1t_2(t_1+t_2)(\alpha_1-\alpha_2)\Delta T}{(E_1t_1^2)^2+(E_2t_2^2)^2+2E_1E_2t_1t_2(2t_1^2+3t_1t_2+2t_2^2)} \quad (2)$$

$$\frac{1}{r} = \frac{6t_1t_2(t_1+t_2)(\alpha_1-\alpha_2)\Delta T}{t_1^4+t_2^4+2t_1t_2(2t_1^2+3t_1t_2+2t_2^2)} \quad (3)$$

Actuators based on graphene/G-O papers can potentially be used in various applications. In the present work, we fabricated "artificial cilia" that may be used to move objects and control positions precisely in a 2-D plane. In another design, eight U-shaped beams were rowed up. The beams were divided into two groups A and B (Fig. 4). Fig. 4 (left column, schematic design; right column, corresponding objects of the artificial cilia) demonstrates the workflow of a moving cycle. Briefly, all beams initially curl up to lift the object when the voltage source corresponding to $U_A = 24$ V and $U_B = 24$ V is turned on (Fig. 4b). Then, the voltage in group B is lowered to 11 V, causing the beams in group B to fall ($U_A = 24$ V, $U_B = 11$ V, Fig. 4c). Next, the voltage in group A is decreased and switched off, causing the object (300 mg) to move over a distance corresponding to $U_A =$ 11 V and $U_B = 11$ V (Fig. 4d). The voltage in group B is then increased to lift the object while moving it farther away (Fig. 4e, corresponding to $U_A = 11$ V and $U_B = 24$ V). Finally, the voltage in group A is increased (Fig. 4f, corresponding to $U_A = 24$ V and $U_B = 24$ V), and the cycle of movement is completed. Comparing Fig. 4b and f, the object may be moved over a significant distance within one cycle; in the present study, for example, a displacement of 9 mm was obtained. In general, the vertical

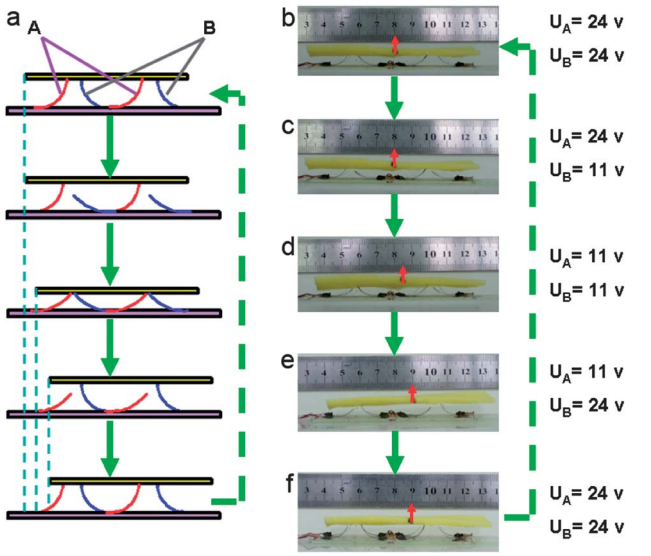

Fig. 4 The workflow of the artificial cilia. The U-shaped beams can be rowed up to form the "cilia," which can be used to move objects precisely. Left: schematic of the artificial cilia; right: the pre-fabricated artificial cilia. Objects can be moved to a distance of up to 9 mm in one cycle.

movement of objects can be realized simply by controlling the voltage applied to the device. To move objects horizontally, the cycle stated above only needs to be repeated. In addition, the length of movement per cycle can be adjusted by varying U_A and U_B. By controlling different groups of actuators, the conversion of electrical power into mechanical movement could be realized, which is of great importance in MEMS applications. It is noteworthy that the object is supported using just 8 beams, which demonstrates that this conveyer system has a high load capacity. Through normalization, it is easily found that the load capacity is up to ~10 mg per actuator, which is at least 50 times higher than that of other conveyer systems (0.196 mg per actuator; 0.022 mg per actuator).[32,33]

Conclusions

A novel actuator based on graphene/G-O papers was fabricated *via* a feasible method, and further to be used for constructing artificial cilia to realize controllable movements of objects in a 2-D plane because of the linear relationship between displacement and voltages. The thermal stress originating from the difference in the coefficients of thermal expansion of the two papers was found to be responsible for the bending of the beams. The tiny artificial cilia show good durability and stability, and are believed to be useful for transporting and moving objects as well as for precise positioning in MEMS/NEMS applications.

Experimental

Preparation of graphite oxide

Graphite oxide was prepared following a modified Hummers method.[42] While maintaining agitation, expandable graphite powder (2 g) and sodium nitrate (1 g) were mixed with sulfuric

acid (46 mL, 98 wt%) in an ice bath. Potassium permanganate (6 g) was slowly added to the mixture to prevent the temperature from exceeding 293 K. The reaction was kept at (308 ± 1) K for 8 h with gas release, after which deionized water (92 mL) was added carefully; this step brought about violent effervescence. The temperature of the water bath was increased to 371 K, and the reaction was allowed to continue for another 15 min to increase the oxidation degree of the graphite oxide product. The resultant bright-yellow suspension was diluted with deionized water (280 mL) and further treated with a solution of H_2O_2 (6 mL, 30%). The intermediate was separated by centrifugation and washed with 5% hydrochloric acid solution seven times until the sulfate could not be detected by $BaCl_2$. The precipitates were washed another seven times with distilled water to remove chloride ions. Finally, the graphite oxide was dried overnight in an airflow drier at 333 K.

Preparation of graphene dispersion

The as-obtained graphite oxide (25 mg) was redispersed in deionized water (70 mL) and exfoliated to generate G-O nanosheets by ultrasonication. While maintaining agitation, hydrazine monohydrate (0.35 mL, as a reductant) and ammonia solution (1.04 mL, for pH adjustment) were added to the nanosheets. The temperature of the mixture solution was kept at 368 K for 1 h in an oil bath, during which the color of the solution gradually changed to dark black, indicating that dispersed G-O nanosheets were reduced to graphene. The dispersion was centrifuged for 30 min at 3000 rpm to remove the precipitate (composed mainly of a fraction of the bulky graphite and an aggregation of graphene). The supernatant of the graphene nanosheet dispersion was carefully poured out. This liquid can be stored in vials for long periods of time without deterioration in quality.

Acknowledgements

This work was supported by the National Basic Research Program of China (Grant no. 2011CB707601 and no. 2009CB623702), the National Natural Science Foundation of China (no. 61274114, 51071044, 61006011, 11204034 and 61106055), Natural Science Foundation of Jiangsu Province (BK2012024, BK2012123), and Scientific Research Foundation of Graduate School of Southeast University (no. YBJJ1208).

References

1 K. Novoselov, A. Geim, S. Morozov, D. Jiang, Y. Zhang, S. Dubonos, I. Grigorieva and A. Firsov, *Science*, 2004, **306**, 666.
2 Y. Zhang, Y. W. Tan, H. L. Stormer and P. Kim, *Nature*, 2005, **438**, 201.
3 X. L. Li, G. Y. Zhang, X. D. Bai, X. M. Sun, X. R. Wang, E. G. Wang and H. J. Dai, *Nat. Nanotechnol.*, 2008, **3**, 538.
4 (*a*) X. Huang and S. L. Zhang, *Modell. Simul. Mater. Sci. Eng.*, 2011, **19**, 054004; (*b*) X. Huang, X. Y. Qi, F. Boey and H. Zhang, *Chem. Soc. Rev.*, 2012, **41**, 666; (*c*) X. Huang, Z. Y. Zeng, Z. X. Fan, J. Q. Liu and H. Zhang, *Adv. Mater.*, 2012, **24**, 5979; (*d*) Q. Y. He, S. X. Wu, Z. Y. Yin and H. Zhang, *Chem. Sci.*, 2012, **3**, 1764; (*e*) X. Huang, Z. Y. Yin, S. X. Wu, X. Y. Qi, Q. Y. He, Q. C. Zhang, Q. Y. Yan, F. Boey and H. Zhang, *Small*, 2011, **7**, 1876.
5 A. R. Ranjbartoreh, B. Wang, X. P. Shen and G. X. Wang, *J. Appl. Phys.*, 2011, **109**, 014306.
6 H. Q. Chen, M. B. Mller, K. J. Gilmore, G. G. Wallace and D. Li, *Adv. Mater.*, 2008, **20**, 3557.
7 O. C. Compton and S. T. Nguyen, *Small*, 2010, **6**, 711.
8 J. W. Suk, R. D. Piner, J. An and R. S. Ruoff, *ACS Nano*, 2010, **4**, 6557.
9 D. A. Dikin, S. Stankovich, E. J. Zimney, R. D. Piner, G. H. B. Dommett, G. Evmenenko, S. T. Nguyen and R. S. Ruoff, *Nature*, 2009, **448**, 457.
10 G. W. Rogers and J. Z. Liu, *J. Am. Chem. Soc.*, 2011, **133**, 10858.
11 J. J. Liang, Y. Huang, J. Y. Oh, M. Kozlov, D. Sui, S. L. Fang, R. H. Baughman, Y. F. Ma and Y. S. Chen, *Adv. Funct. Mater.*, 2011, **21**, 3778.
12 K. Y. Shin, J. Y. Hong and J. Jang, *Chem. Commun.*, 2011, **47**, 8527.
13 J. H. Jung, J. H. Jeon, V. Sridhar and I. K. Oh, *Carbon*, 2011, **49**, 1279.
14 N. N. Zhang, R. Q. Li, L. Zhang, H. B. Chen, W. C. Wang, Y. Liu, T. Wu, X. D. Wang, W. Wang, Y. Li, Y. Zhao and J. P. Guo, *Soft Matter*, 2011, **7**, 7231.
15 Y. F. Lian, Y. X. Liu, T. Jiang, J. Shu, H. Q. Lian and M. H. Cao, *J. Phys. Chem. C*, 2010, **114**, 9659.
16 J. J. Liang, Y. F. Xu, Y. Huang, L. Zhang, Y. Wang, Y. F. Ma, F. F. Li, T. Y. Guo and Y. S. Chen, *J. Phys. Chem. C*, 2009, **113**, 9921.
17 S. E. Zhu, R. Shabani, J. Rho, Y. Kim, B. H. Hong, J. H. Ahn and H. J. Cho, *Nano Lett.*, 2011, **11**, 977.
18 S. J. Park, J. H. An, J. W. Suk and R. S. Ruoff, *Small*, 2009, **6**, 210.
19 X. J. Xie, L. T. Qu, C. Zhou, Y. Li, J. Zhu, H. Bai, G. Q. Shi and L. M. Dai, *ACS Nano*, 2010, **4**, 6050.
20 C. Y. Li and T. W. Chou, *Appl. Phys. Lett.*, 2006, **89**, 063103.
21 P. Kim and C. M. Lieber, *Science*, 1999, **286**, 2148.
22 J. Lee and S. Kim, *Sens. Actuators, A*, 2005, **120**, 193.
23 T. Rueckes, K. Kim, E. Joselevich, G. Y. Tseng, C. L. Cheung and C. M. Lieber, *Science*, 2000, **289**, 94.
24 L. Forró, *Science*, 2000, **289**, 560.
25 V. V. Deshpande, H. Y. Chiu, H. W. C. Postma, C. Miko, L. Forró and M. Bockrath, *Nano Lett.*, 2006, **6**, 1092.
26 N. Bassik, B. T. Abebe, K. E. Laflin and D. H. Gracias, *Polymer*, 2010, **51**, 6093.
27 U. L. Zainudeen, M. A. Careen and S. Skaarup, *Sens. Actuators, B*, 2008, **134**, 467.
28 R. Techapiesancharoenkij, J. Kostamo, S. M. Allen and R. C. O'Handley, *J. Magn. Magn. Mater.*, 2011, **323**, 3109.
29 K. Tsiakmakis and T. Laopoulos, *Meas. Sci. Technol.*, 2011, **22**, 114006.
30 Y. Chida, H. Katsumata, T. Fujiya, S. Kaihatsu, T. Morita, D. Hoshino and Y. Nishioka, *Sens. Actuators, A*, 2011, **169**, 367.

31 L. H. Lu, J. H. Liu, Y. Hu, Y. W. Zhang and W. Chen, *Adv. Mater.*, 2013, **25**, 1270.
32 C. T. Wu and W. Y. Hsu, *Microsyst. Technol.*, 2006, **12**, 293.
33 Y. A. Chapuis, Y. Fukuta, Y. Mita and H. Fujita, *Proc. SPIE–Int. Soc. Opt. Eng.*, 2004, **5389**, 355.
34 Q. Z. Liang, X. X. Yao, W. Wang, Y. Liu and C. P. Wong, *ACS Nano*, 2011, **5**, 2392.
35 S. Kim, S. Zhou, Y. K. Hu, M. Acik, Y. J. Chabal, C. Berger, W. de Heer, A. Bongiorno and E. Riedo, *Nat. Mater.*, 2012, **11**, 544.
36 C. Y. Li and T. W. Chou, *Appl. Phys. Lett.*, 2006, **89**, 063103.
37 S. K. Lee, H. Y. Jang, S. Jang, E. Choi, B. H. Hong, J. Lee, S. Park and J. H. Ahn, *Nano Lett.*, 2012, **12**, 3472.
38 H. Y. Jeong, J. Y. Kim, J. W. Kim, J. O. Hwang, J. E. Kim, J. Y. Lee, T. H. Yoon, B. J. Cho, S. O. Kim, R. S. Ruoff and S. Y. Choi, *Nano Lett.*, 2010, **10**, 4381.
39 Q. Y. He, H. G. Sudibya, Z. Y. Yin, S. X. Wu, H. Li, F. Boey, W. Huang, P. Chen and H. Zhang, *ACS Nano*, 2010, **4**, 3201.
40 S. Timoshenko, *J. Opt. Soc. Am.*, 1925, **11**, 233.
41 C. Liu, Foundations of MEMS, Prentice Hall, 2007, ISBN-10:0131472860.
42 W. S. Hummers and R. E. Offeman, *J. Am. Chem. Soc.*, 1958, **80**, 1339.